iScience

CellPress
OPEN ACCESS

Article

Thyroid hormone treatment counteracts cellular phenotypical remodeling in diabetic organs

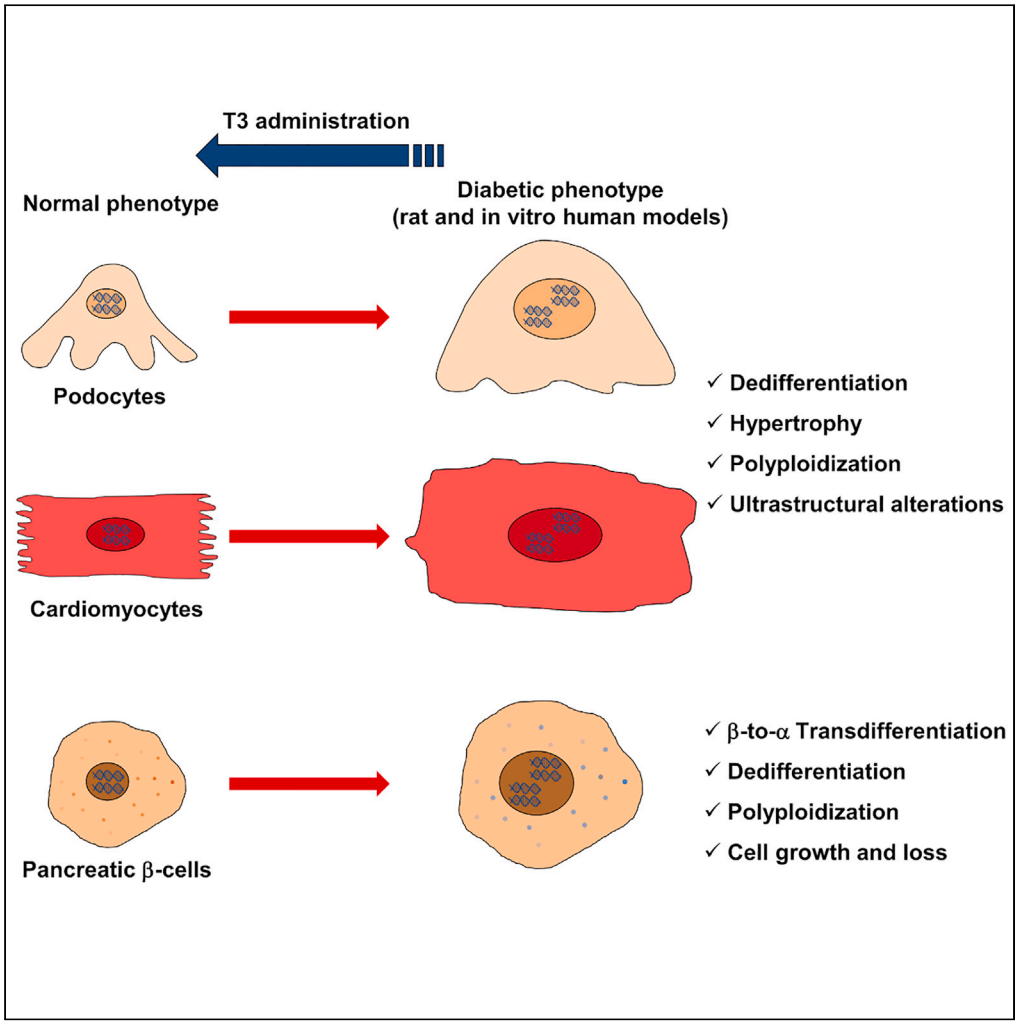

Angelo M. Lavecchia, Polyxeni Mantzouratou, Domenico Cerullo, ..., Carlamaria Zoja, Giuseppe Remuzzi, Christodoulos Xinaris

christodoulos.xinaris@marionegri.it

Highlights

TH signaling controls major phenotypical alterations in diabetic organs and organoids

T3 reverses diabetes-induced pathological remodeling in cardiomyocytes and podocytes

T3 prevents transdifferentiation, growth, and loss in diabetic pancreatic beta cells

T3 treatment provides a new therapeutic approach for diabetes and its complications

Lavecchia et al., iScience 26, 107826
October 20, 2023
https://doi.org/10.1016/j.isci.2023.107826

iScience

CellPress
OPEN ACCESS

Article

Thyroid hormone treatment counteracts cellular phenotypical remodeling in diabetic organs

Angelo M. Lavecchia,[1,2] Polyxeni Mantzouratou,[1,2] Domenico Cerullo,[1] Monica Locatelli,[1] Sara Conti,[1] Matteo Tironi,[1] Fabio Sangalli,[1] Daniela Corna,[1] Carlamaria Zoja,[1] Giuseppe Remuzzi,[1] and Christodoulos Xinaris[1,3,*]

SUMMARY

Diabetes mellitus and alterations in thyroid hormone (TH) signaling are closely linked. Though the role of TH signaling in cell differentiation and growth is well known, it remains unclear whether its alterations contribute to the pathobiology of diabetic cells. Here, we aim to investigate whether the administration of exogenous T3 can counteract the cellular remodeling that occurs in diabetic cardiomyocytes, podocytes, and pancreatic beta cells.

Treating diabetic rats with T3 prevents dedifferentiation, pathological growth, and ultrastructural alterations in podocytes and cardiomyocytes. *In vitro*, T3 reverses glucose-induced growth in human podocytes and cardiomyocytes, restores cardiomyocyte cytoarchitecture, and reverses pathological alterations in kidney and cardiac organoids. Finally, T3 treatment counteracts glucose-induced transdifferentiation, cell growth, and loss in pancreatic beta cells through TH receptor alpha1 activation. Our studies indicate that TH signaling activation substantially counteracts diabetes-induced pathological remodeling, and provide a potential therapeutic approach for the treatment of diabetes and its complications.

INTRODUCTION

Diabetes is one of the biggest health emergencies of the 21st century. It affects over 425 million people worldwide, kills 3 people every minute, and costs over $825 billion per year.[1] Two-thirds of these deaths are due to diabetic nephropathy (DN) and diabetic cardiomyopathy: DN develops in approximately 40% of diabetic patients[2] and cardiovascular disease is the most prevalent cause of morbidity and mortality in diabetic patients.[3] Although standard treatments such as glucose-lowering medications[4] and renin-angiotensin system blockade[5,6] can partially delay organ damage,[7–9] there is currently no definitive cure for diabetes and its complications.

One of the main limitations to the development of such therapies has been the complex mechanistic pathobiology of diabetic organs. First, during chronic injury, terminally differentiated and highly specialized cells of complex organs (i.e., podocytes,[10] cardiomyocytes,[11] and pancreatic beta cells[12]) dedifferentiate, undergo cytoarchitectural reorganization, and simultaneously reactivate numerous fetal genes that control cellular structure and function. Second, dedifferentiating cells re-enter the cell cycle, replicate their DNA, and grow in size, but being unable to conclude mitosis, remain polyploid and hypertrophic. While these profound cellular changes (defined as cellular remodeling) are necessary to save energy and compensate for tissue loss, hypertrophied cells biophysically perform with sub-optimal metabolism and viability and eventually fail to preserve homeostasis and functionality.[13–15] Although many aspects of cellular remodeling are known in diabetes, little is known about the molecular pathway(s) that coordinate these processes.

Two decades of research (by us[10,16–18] and others[19,20]) have shown that thyroid hormone (TH) signaling—in addition to its critical role in physiological growth and organ development—plays similar roles in conditions that encompass cellular dedifferentiation, cytoarchitectural reorganization, and compensatory growth. In response to various stressful stimuli, T3 levels drop and the TH nuclear receptor alpha1 (TRα1) switches to its unliganded aporeceptor state to induce cell dedifferentiation, the reactivation of fetal genes, and cell growth. This recapitulation of the fetal pattern of TH signaling, which has been extensively studied in myocardial infarction, is thought to play a crucial role in pathological ventricular remodeling and the development of heart failure.[21,22] It is of great interest that TH signaling is severely altered at various levels in diabetes: diabetic patients have significantly lower T3 plasma levels[23] and overexpress TRα1 in podocytes,[10] while in cardiomyocytes a number of TH-dependent fetal and adult genes are upregulated and downregulated, respectively.[24]

Nevertheless, despite the well-documented alterations in TH signaling in diabetes, it remains unclear whether the reduction of TH levels is related to the pathogenesis and/or adaptive repair of diabetic organs, or is merely a secondary effect caused by diabetes stress. Moreover, it

[1]Istituto di Ricerche Farmacologiche Mario Negri IRCCS, Centro Anna Maria Astori, Science and Technology Park Kilometro Rosso, Via Stezzano 87 -, 24126 Bergamo, Italy
[2]These authors contributed equally
[3]Lead contact
*Correspondence: christodoulos.xinaris@marionegri.it
https://doi.org/10.1016/j.isci.2023.107826

is not known whether TH signaling could play a direct role in the pathobiology of the diabetic pancreas *per se*, or whether its modulation could prevent or reverse cellular remodeling in diabetes.

Here, we aimed to determine whether the administration of exogenous T3 could prevent the cellular remodeling of three highly specialized cell types that are crucially affected by diabetes: cardiomyocytes, podocytes, and pancreatic cells.

RESULTS

T3 treatment prevents fetal gene reactivation and pathological alterations in the diabetic kidney and heart

To test whether TH administration can counteract diabetes-induced alterations in TH signaling and subsequent reactivation of fetal gene in the kidney and heart,[25,26] we treated Zucker diabetic fatty (ZDF) rats with T3 and evaluated changes in TH signaling at the systemic and tissue levels. As expected,[10] the blood levels of the active forms of THs were significantly lower in diabetic rats than in lean control animals (Figures S1A–S1C). The expression of the key enzyme that locally maintains low levels of T3 during early development—type III iodothyronine deiodinase (DIO3)—increased significantly in the glomeruli and hearts of diabetic animals (Figures 1A and 1B). In the diabetic kidney, TRα1 levels were also significantly higher in glomerular cells, whereas cardiac TRα1 was highly expressed in all groups (Figures 1C and 1D). Notably, treatment with T3, although did not affect T3 serum levels (Figure S1A), reversed the previously described changes by normalizing TRα1 in the kidney and decreasing both glomerular and cardiac DIO3 (Figure 1).

To assess whether the availability of TH could affect the differentiation status of podocytes and cardiomyocytes in diabetes, we evaluated the expression of fetal markers in kidney and heart specimens from control, vehicle-, and T3-treated animals. As previously observed in ZDF rats and other animal models of diabetes,[10] classic fetal kidney markers (Pax2, Six2) were upregulated in podocytes of diabetic rats (Figures 1E and 1F). Likewise, diabetic hearts exhibited an upregulation of the ratio between β and total myosin heavy chain (Figure 1G) and concomitant downregulation of the ratio between SERCA2a and PLN compared to lean rats (Figure 1H), indicating a switch to the fetal cardiomyocyte contraction profile.[26] Again, treatment with T3 prevented the upregulation of the fetal kidney markers and cardiac β myosin and almost normalized the SERCA2a to PLN ratio (Figures 1E–1H).

In addition to maintaining the normal cellular phenotype, T3 significantly reduced glomerulosclerosis (Figure 2A), as well as the expression of desmin in podocytes and α-SMA in the glomeruli, indicating a reduction in podocyte dedifferentiation and glomerular fibrosis, respectively (Figures 2B and 2C). Likewise, histological analysis of Sirius red staining of the heart showed extensive fibrosis in vehicle-treated ZDF animals, which was markedly reduced by T3 treatment (Figure 2D).

Finally, to assess whether T3 could exert similar effects in human tissues, we studied the effect of T3 on glucose-injured kidney (Figures 2E, S1D, and S1E) and cardiac (Figures 2F, S1F, and S1G, and Video S1) organoids. Remarkably, T3 treatment strongly counteracted the expression of classic diabetes injury and fibrosis markers in human podocytes and cardiomyocytes (Figures 2E, 2F, S1F, and S1G), further confirming the central role of TH signaling in maintaining the normal cellular phenotype during glucose injury.

Thyroid hormone administration counteracts pathological growth in diabetic podocytes and cardiomyocytes and maintains cardiomyocyte cytoarchitecture

Apart from cell dedifferentiation, which can negatively affect homeostasis, in complex cells both size and architecture are implicitly and linearly correlated with cell functionality and viability.[13–15] To assess whether TH signaling plays a role in cell enlargement (hypertrophy), we performed morphometric studies in diabetic animals and human cell models after T3 treatment. Diabetic rats exhibited increased podocyte volume, measured as the percentage of the area that was positive for Glepp1—a marker of podocyte apical cell membrane—and a decrease in podocyte number, measured as the number of Wilm's tumor 1-positive podocytes per glomerulus, compared to lean rats (Figures 3A and 3B). Interestingly, T3 treatment significantly reduced podocyte volume and rescued podocyte number in diabetic rats (Figures 3A and 3B). Consistent with this, the Feret's diameter of cardiomyocytes significantly increased in diabetic rats compared to lean controls, while treatment with T3 totally restored the normal cardiomyocyte architecture (Figures 3C and S1H).

Pathological growth can encompass both hypertrophy and polyploidy. To determine whether TH signaling plays a role in polyploidization, we quantitatively analyzed and compared the nuclear DNA content of glomerular cells and cardiomyocytes from lean, vehicle-, and T3-treated ZDF animals (Figures 3D and 3E) by using Z-stacking and 3D reconstructions of thick histological sections[27] (Figure 3F). In untreated ZDF animals, the DNA content of both glomerular cells and cardiomyocytes was significantly higher than in lean rats, whereas T3 treatment completely normalized the DNA content in these cells (Figures 3D and 3E).

Consistent with the animal studies, human *in vitro* models of high glucose injury showed that both podocytes and cardiomyocytes exhibited a significant increase in average surface area after high glucose injury, whereas T3 reversed this response (Figures 3G and 3H). Cultured cardiomyocytes stressed with high glucose concentration not only had a larger cell area but also adopted a "fetal-like" round shape[28,29] which was normalized by T3 treatment (Figure 3I).

Thyroid hormone treatment preserves renal and cardiac ultrastructure

To investigate in greater depth the effect that T3 treatment has on the ultrastructural phenotype of podocytes and cardiomyocytes, we analyzed tissues from lean, vehicle-, and T3-treated diabetic animals, using both transmission electron microscopy (TEM) and SEM (Figure 4). TEM showed that, in ZDF rats, glomerular ultrastructural integrity was highly subverted (Figure 4A). Specifically, severe degeneration of the podocyte cytoarchitecture was observed in ZDF rats compared to lean animals with almost complete foot process effacement (Figure 4A,

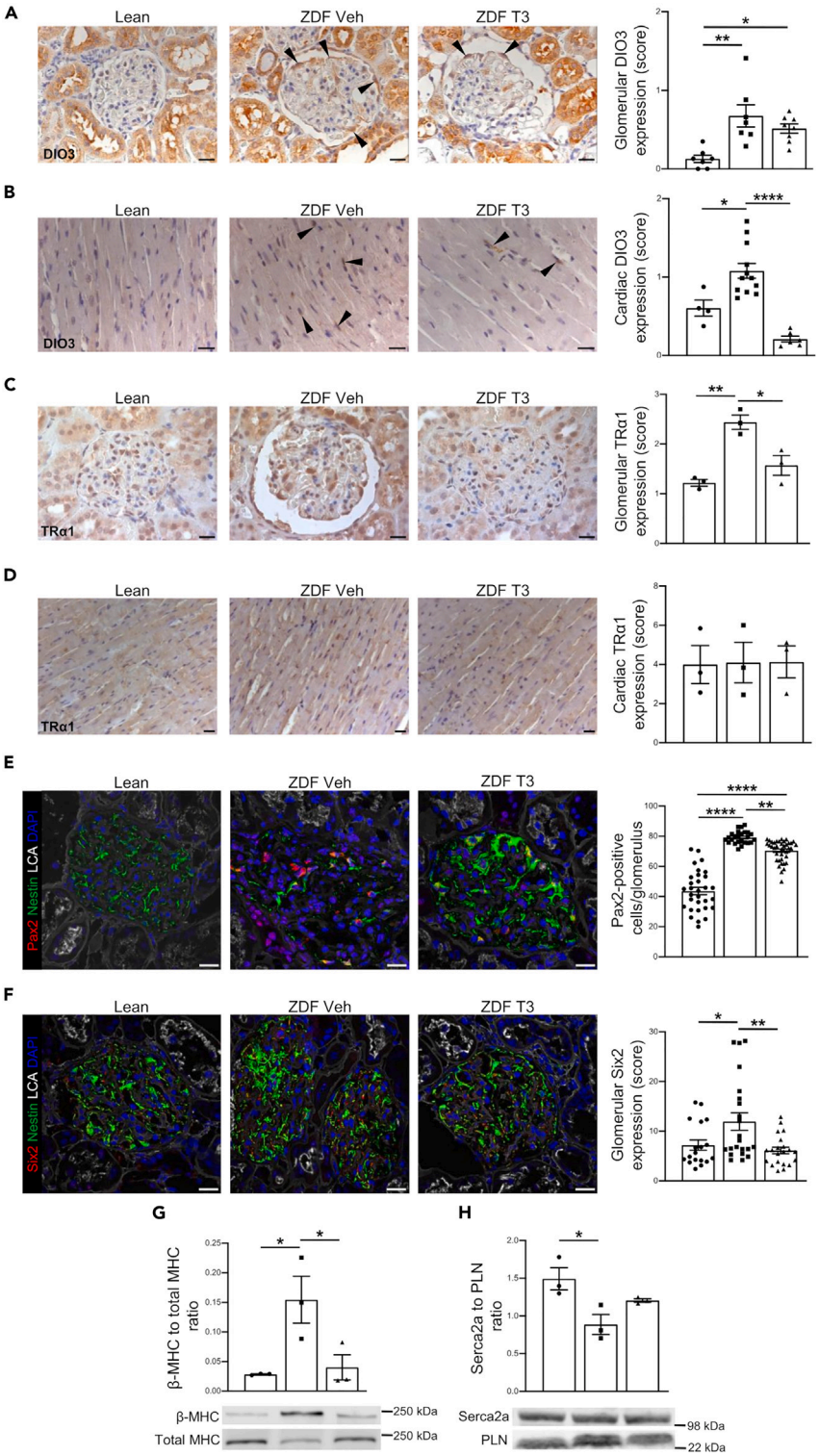

Figure 1. Treatment with T3 restores the TH signaling expression profile and prevents fetal gene reactivation in the diabetic kidney and heart

(A and B) Representative images (left panels) and quantification (right panel) of DIO3 expression in glomeruli (A) and left ventricle (B) specimens of lean and ZDF rats. (C and D) Representative images (left panels) and quantification (right panel) of TRα1 expression in glomeruli (C) and left ventricle (D) of lean and diabetic animals. (E and F) Representative images of nestin-positive podocytes expressing Pax2 (E, left) and Six2 (F, left) in renal sections of lean and ZDF rats. Quantification of Pax2-positive cells (E, right) and Six2 expression (F, right) in glomeruli of lean and diabetic animals.

Figure 1. *Continued*

(G and H) Densitometric analysis and western blot of beta-to-total MHC (G) and SERCA2a to phospholamban (H) ratio in left ventricle of lean and ZDF rats. Data are expressed as mean ± SEM, one-way ANOVA corrected with Tukey's post hoc test. *p < 0.05, **p < 0.01, ****p < 0.0001. n = 3–8 rats per group. Scale bars, 20 μm. LCA, *Lens culinaris agglutinin*. Black circles: Lean; black squares: ZDF Veh; black triangles: ZDF T3.

arrows in high magnification insets), loss of endothelial fenestration (Figure 4A, white arrowhead), the presence of large vacuoles in the cytosol of podocytes (Figure 4A, red asterisk), and mitochondrial swelling and cristae fragmentation (Figure 4A, red arrowhead). SEM analysis confirmed the TEM observations and showed that changes in ZDF rats were obviously ameliorated by T3 treatment (Figure 4B). In particular, unlike lean animals, ZDF rats exhibit effacement of the interdigitating foot processes (Figure 4B, asterisks), podocyte cell body attenuation, and expansion of the area covered by the podocyte body. In contrast to the untreated animals, diabetic rats treated with T3 displayed typically well-preserved glomeruli, good preservation of the podocyte cytoarchitecture, and reduced effacement of the interdigitating foot processes (Figure 4B).

Regarding heart morphology, TEM showed that cardiomyocyte structural integrity in ZDF rats was dramatically impaired compared to lean rats. Cellular damage was characterized by diffuse mitochondrial swelling and cristae fragmentation (Figure 4C, arrowheads), myofibril disruption (Figure 4C, red asterisks), and Z line disappearance (Figure 4C, arrows). Treatment with T3 almost totally reversed these alterations (Figure 4C). SEM images confirmed the TEM analysis, demonstrating that in ZDF rats, mitochondrial swelling and the Z line disappearance were obvious, compared to the conserved morphology observed in lean rats (Figures 4D and 4E). These alterations were less pronounced in T3-treated diabetic rats (Figures 4D and 4E), further confirming that T3 treatment strongly protects cardiomyocyte structure and tissue integrity.

T3 treatment counteracts dedifferentiation and transdifferentiation of beta cells in diabetic rats

Although until recently the loss of functional beta cells was thought to be mainly due to apoptosis, there is now growing evidence that beta cells respond to stress by dedifferentiating or transdifferentiating into other cell types, i.e., alpha-like glucagon-producing cells.[12]

To evaluate the role of TH signaling in beta pancreatic cell dedifferentiation, we analyzed the expression PDX1 and NKX6.1—normally expressed in terminally differentiated beta cells and downregulated in response to diabetic injury[30]—in pancreatic specimens from lean and vehicle- or T3-treated ZDF rats. Immunofluorescence analysis showed that nuclear expression of both PDX1 and NKX6.1 was downregulated with a concurrent translocation to the cytoplasm (Figures S2A and S2B). This observation was further confirmed by western blot quantitative analysis, which showed a significant reduction of PDX1 and NKX6.1 nuclear levels in diabetic animals (Figures S2A and S2B). Remarkably, T3 treatment counteracts these responses by restoring PDX1 and NKX6.1 localization and almost normalizing their nuclear expression levels (Figures S2A and S2B).

To assess the role that TH signaling plays in beta pancreatic cell transdifferentiation into alpha cells, we co-immunostained isolated pancreata with (i) synaptophysin (a marker of endocrine cells) and insulin or glucagon, or (ii) with insulin and glucagon together (Figures 5A–5C). Then the area positive for insulin or glucagon was quantified and expressed against the total area of pancreatic islet (Figures 5A and 5B). Also, the numbers of bihormonal on total cells numbers were quantified in all the groups (Figure 5C). The results showed that diabetic animals exhibited a robust decrease of the insulin-secreting area (Figure 5A) accompanied by a remarkable increase of glucagon-secreting cells (Figure 5B). Also, the number of bihormonal cells rose significantly, suggesting that insulin-producing beta cells in ZDF animals transdifferentiate into glucagon-producing alpha cells (Figure 5C). Notably, treatment with T3 significantly increased the insulin-secreting area (Figure 5A), significantly decreased the glucagon area to control levels (Figure 5B), and restored the number of bihormonal cells (Figure 5C).

T3 administration prevents beta cell polyploidization and preserves islet structure and function

To assess whether beta cells undergo polyploidization in response to diabetes and the possible role of TH signaling in this process, we quantitatively analyzed their nuclear DNA content (Figure S2C). Interestingly, the DNA content in insulin-secreting cells from diabetic animals increased significantly compared to lean rats, while T3 treatment normalized DNA content to control levels (Figure S2C).

Given that both hyperglycemic injury and polyploidy are associated with increased apoptosis,[31] we performed immunofluorescence analysis for cleaved caspase-3—an apoptosis marker—on pancreatic tissue from lean and ZDF rats (Figure S2D). In fact, compared to control rats, vehicle-treated ZDF animals displayed a significant increase of apoptosis in pancreatic beta cells, while the treatment with T3 counteracted this response (Figure S2D).

To further study the effect of T3 on pancreatic islet architecture—which is crucial for maintaining islet function[32]—we performed Masson's trichrome staining on pancreatic specimens from lean and diabetic animals and evaluated collagen fiber distribution around pancreatic islets (Figure S2E). Histological analysis of the pancreatic sections showed that collagen fiber distribution was significantly altered in the pancreatic islets of untreated diabetic rats compared to lean animals. Interestingly, treatment with T3 ameliorated the disorganization of the pancreatic islet and restored the normal distribution of collagen fibers around the islet (Figure S2E). Accordingly, the T3 serum levels strongly correlated with glucose levels in ZDF rats, suggesting that treatment with T3 protects pancreatic function (Figure S2F).

T3-TRα1 axis controls pancreatic beta cell transdifferentiation and pathological growth in human diabetes models

To assess whether TH signaling plays a role in pathological changes in human pancreatic beta cells, we exposed purified human beta cells to high concentrations of glucose and evaluated phenotypic changes. Results from immunofluorescence analysis (Figures 5D–5H) showed that high glucose injury concurrently induced an increase in glucagon-positive cells and a decrease in intracellular content of insulin, further

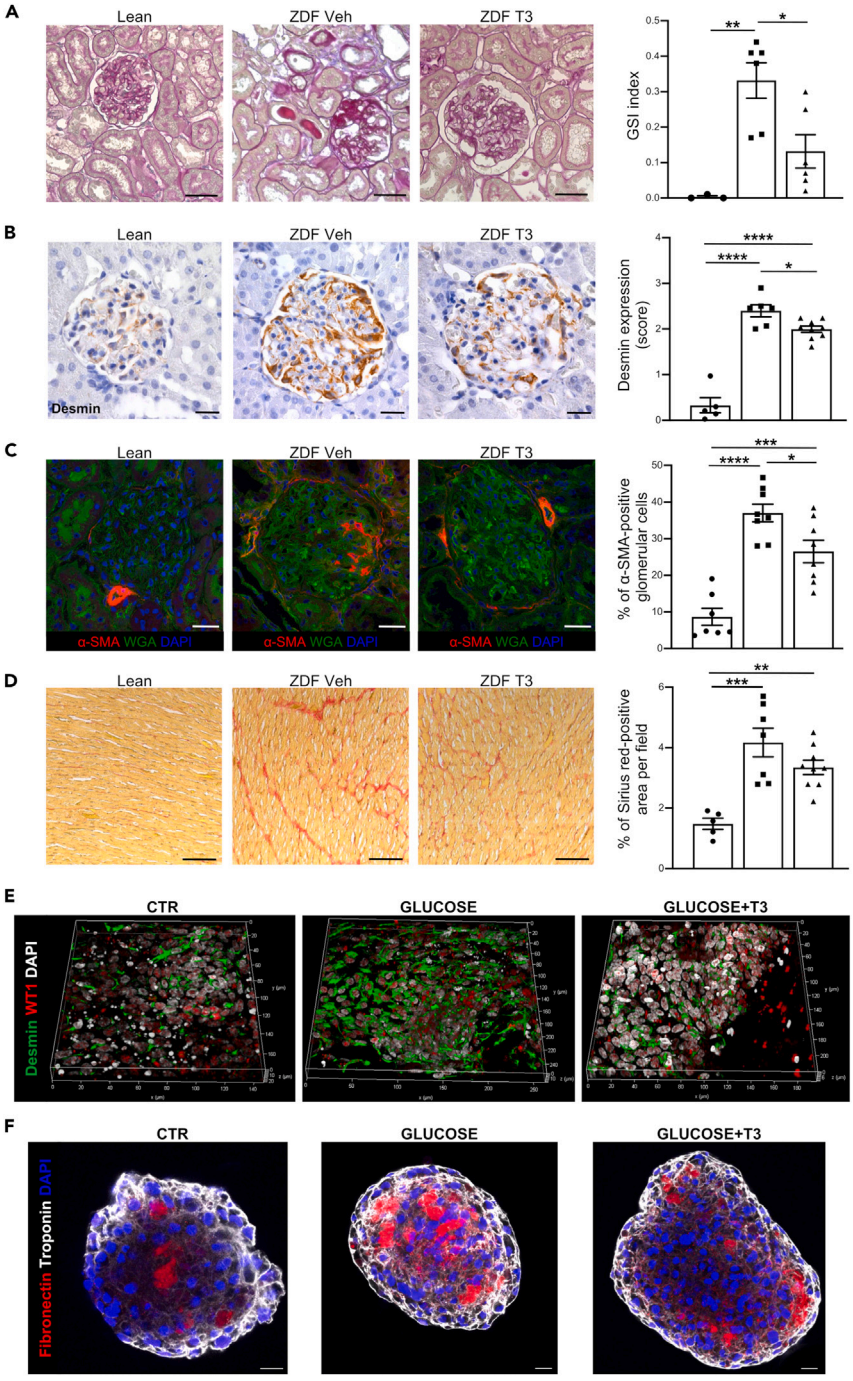

Figure 2. T3 treatment counteracts pathological alterations in both diabetic kidney and heart and in *in vitro* human models of high glucose injury

(A) Representative images from histological PAS staining in lean and ZDF rat kidney sections (left panels) and analysis of glomerulosclerosis index (right panel).

(B and C) Representative images (left panels) and quantification (right panel) of glomerular desmin (B) and α-SMA (C) staining in lean and diabetic animals.

(D) Representative images (left panels) and quantification (right panels) of Sirius red staining in left ventricular tissue of lean and ZDF rats.

(E) Representative images of WT1 and desmin staining in control, glucose-injured, and T3-treated hiPSC-derived kidney organoids.

(F) Representative images of fibronectin and troponin staining in control, glucose-injured, and T3-treated hiPSC-derived cardiac organoids. Data are expressed as mean ± SEM, one-way ANOVA corrected with Tukey's post hoc test. *$p < 0.05$, **$p < 0.01$, ***$p < 0.001$, ****$p < 0.0001$. n = 3–9 rats per group. Scale bars, 50 μm (A), 20 μm (B, F), 25 μm (C), 100 μm (D). Black circles: Lean; black squares: ZDF Veh; black triangles: ZDF T3.

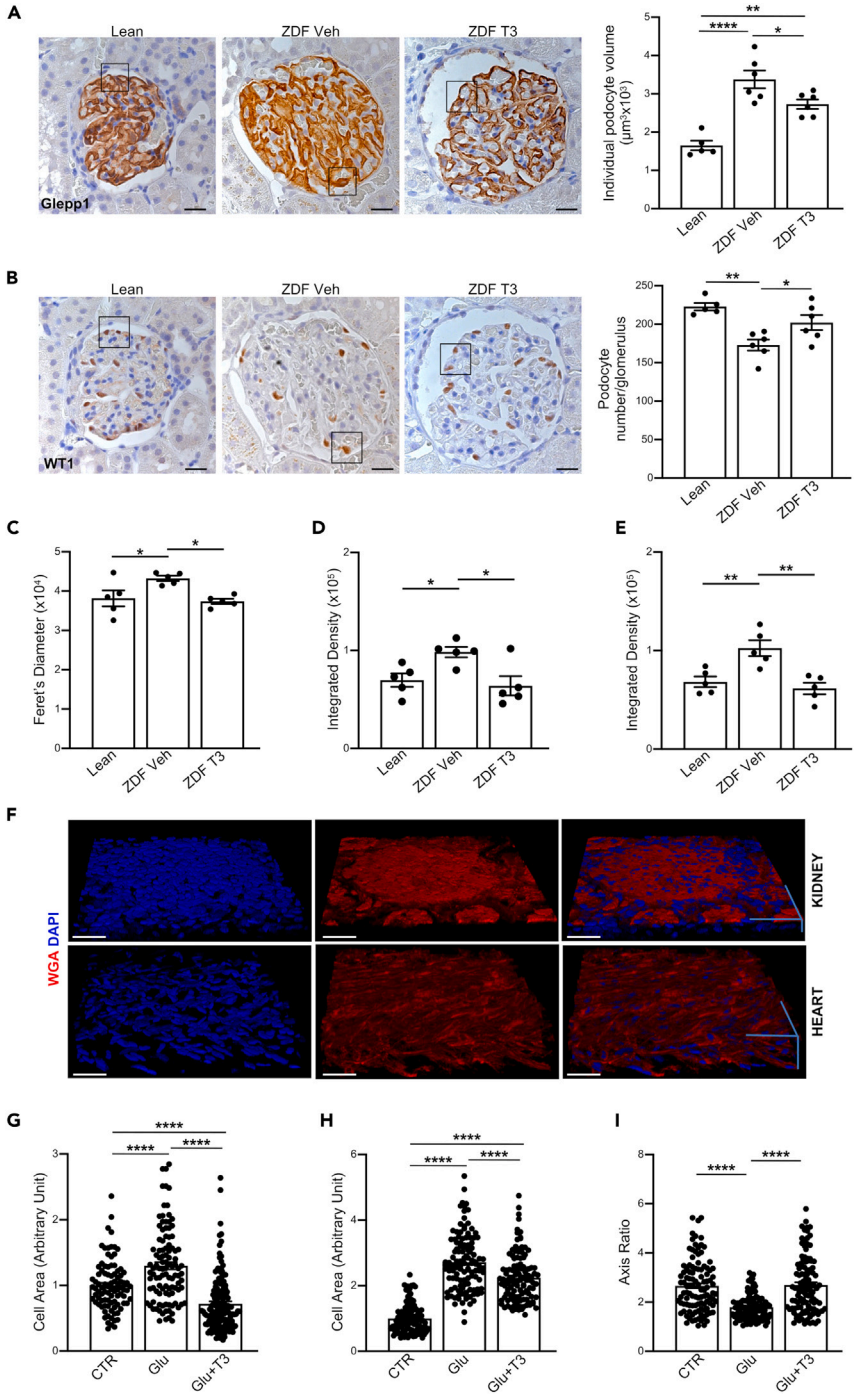

Figure 3. Treatment with T3 counteracts pathological growth in diabetes- and glucose-injured podocytes and cardiomyocytes and maintains cardiomyocytes cytoarchitecture

(A and B) Representative images of Glepp1 (A) and WT1 (B) staining in kidney serial sections of lean and diabetic animals. Quantification of individual podocyte volume and WT1-positive podocytes in lean and ZDF rats (A and B, right).

(C) Quantification of Feret's diameter in cardiomyocytes.

(D and E) Evaluation of DNA content in glomerular cells (D) and cardiomyocytes (E) of control and diabetic animals.

(F) Representative images of 3D reconstructed kidney (top) and heart (bottom) tissue sections. Tissues were stained with rhodamine-labeled WGA lectin.

Figure 3. *Continued*

(G–I) Quantification of cell area (G, H) and axis ratio (I) in control, glucose-injured, and T3-treated human podocytes (G) and cardiomyocytes (H, I). For quantification, representative images were randomly taken from different areas of cell culture. At least 91 cells from each group were analyzed from n = 3 independent experiments (G–I). Data are expressed as mean ± SEM, one-way ANOVA corrected with Tukey's post hoc test. *p < 0.05, **p < 0.01, ****p < 0.0001. n = 5–6 animals per group. Scale bars, 20 μm (A, B), 40 μm (F).

confirming that the high concentration of glucose induces the transdifferentiation of beta into alpha cells (Figures 5E and 5F). Moreover, after high glucose injury, we also observed a significant reduction in the number of cells (Figure 5G) and an increase (though not significant) in cell area (Figure 5H) compared to control cells. Remarkably, treatment with T3 significantly increased intracellular insulin content and decreased the number of transdifferentiating cells, restored cell numbers to the control level, and markedly reduced the pancreatic beta cell area (Figures 5E–5H). Conversely, the inhibition of T3 binding to TRα1 with desbutyl-dronedarone[33]—before adding T3 to glucose-stressed cells—completely abrogated the beneficial effects of T3, and largely enhanced further transdifferentiation of beta cells into alpha cells (Figures 5E–5H). This suggests that the unliganded TRα1 may trigger opposing actions with respect to the liganded receptor in the diabetic pancreas, further highlighting the role of the T3-TRα1 axis in the previously mentioned patho-phenotypical responses.

DISCUSSION

Thyroid hormone signaling is one of the most ancient molecular pathways. In virtually all taxa, it controls metabolism, growth, and development.[25] In diabetes, alterations in TH signaling are some of the most common complications, which manifest as lower T3 plasma levels[23] and thyroid dysfunction (i.e., subclinical and clinical hypothyroidism).[34,35] These alterations have long been considered relatively "innocent" metabolic adaptations to chronic illness, and largely studied under the spectrum of systemic hypothyroidism.

Here, we studied for the first time simultaneously 3 diabetic organs and found that TH signaling plays a central role in the patho-phenotypical remodeling of podocytes, cardiomyocytes, and beta pancreatic cells. Most importantly, our findings show that exogenous administration of T3 can effectively counteract these changes and improve pancreatic function.

Both the kidney and heart of obese diabetic rats displayed a fetal TH signaling profile—which is characterized by high local expression of TRα1 and DIO3[25,26]—probably triggered by low TH availability.[36–38] Considering the actions of TH signaling during early development and tissue regeneration, we have previously proposed that the fetal TH signaling in adult life acts antagonistically, by conferring immediate vital benefits to damaged tissues and then having a late, maladaptive, debilitating effect in the long term.[25,26,39] Here, our data further support this thesis by demonstrating that, at least in diabetes, pathological cellular changes, such as cell dedifferentiation and polyploidy/hypertrophy, are indeed affected by alterations of TH signaling and dependent on T3 availability. In fact, T3 administration exhibited a remarkable ability to maintain normal cellular structure and size and prevent dedifferentiation and pathological growth both in animal and human podocytes and cardiomyocytes.

These actions and underlying mechanisms of TH signaling in podocytes and cardiomyocytes appear to be similar in pancreatic beta cells. A progressively growing body of evidence suggests that TH signaling plays a critical role in the development of the pancreatic islet[40,41] and beta cell proliferation in neonatal rats.[42] Despite this knowledge, the beneficial effects of TH on patients[43,44] and the underlying mechanisms of TH actions in pancreas repair/regeneration remain, respectively, controversial and insufficiently understood. Our findings indicate that T3 administration prevents pathological growth and apoptosis in pancreatic beta cells, ameliorates the structure and organization of the pancreatic islets, and increases insulin expression in an animal model of type II diabetes. Most importantly, our study revealed that TH signaling plays a central role in human beta cell dedifferentiation and beta-to-alpha cell transdifferentiation, both contributing to beta cell mass loss as well as apoptosis.[45,46] Notably, blocking T3 binding to TRα1 with a selective inhibitor worsened high glucose-induced effects on beta cell transdifferentiation. This finding suggests that TRα1 acts as a molecular "switch" that can drive different and opposing functions depending on its liganded state, as happens during the different stages of embryonic development. As such, the modulation of TRα1 in the diabetic pancreas is clinically and therapeutically significant, if managed in a timely manner.

One inherent challenge in translating these findings to clinical practice is how to balance the therapeutic benefits and possible side effects of TH treatment. Here, T3 treatment did result in a persistent downward trend for proteinuria (Figure S3B), as previously shown in short-term treatment of diabetic mice,[47] but this long-term treatment caused a supraphysiologic elevation of glomerular filtration rate (Figure S3C). Another important observation is that, although T3 treatment did not significantly affect hormone's circulating levels, it could still exert its therapeutic and adverse effects at tissue level. Given that the intensity of the treatment is determinant for the clinical outcome,[48,49] the previously described findings should be cautiously taken into consideration by studies that aim to treat diabetic patients on the basis of circulating THs.

Although more focused safety studies remain to be done to exploit clinically the beneficial effects of TH treatment, this study reveals hitherto unknown aspects of TH signaling in the pathogenesis of diabetes and its complications and provides a novel conceptual platform for counteracting debilitation and promoting repair of diabetic organs simultaneously.

Limitation of the study

As discussed previously, strengthening the therapeutic efficacy of T3 treatment on kidney function by using higher doses of T3 was not possible because it caused a supraphysiologic increase (1.29-fold vs. ZDF vehicle) in glomerular filtration—measured as glomerular filtration rate through iohexol plasma clearance (GFR, mL/min/100 g of body weight).

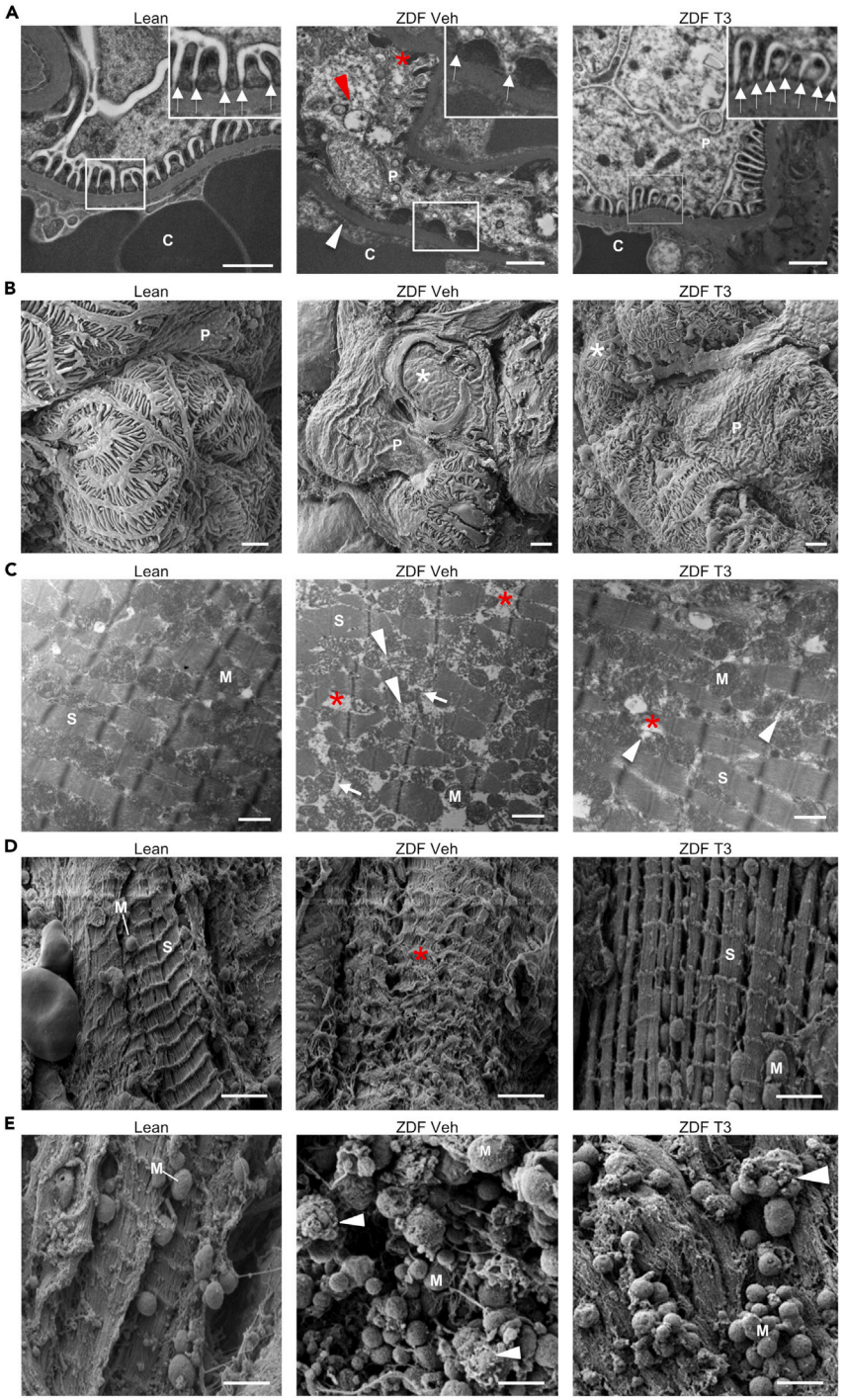

Figure 4. T3 administration preserves glomerular and cardiac ultrastructural integrity in diabetic animals

(A) Representative high-resolution TEM photomicrographs of glomerular capillary barrier, at low and high magnification (insets) from lean and ZDF rats.

(B) Representative SEM photomicrographs of glomerular tuft from lean and ZDF rats.

(C) Representative TEM photomicrographs of left ventricular tissue from lean and ZDF rats.

(D and E) Representative SEM photomicrographs of left ventricular tissue at low (D) and high magnification (E) from lean and diabetic rats. Scale bars, 1 μm (A, C), 2 μm (B, D, E). P, podocyte; C, capillary lumen; M, mitochondria; S, sarcomere.

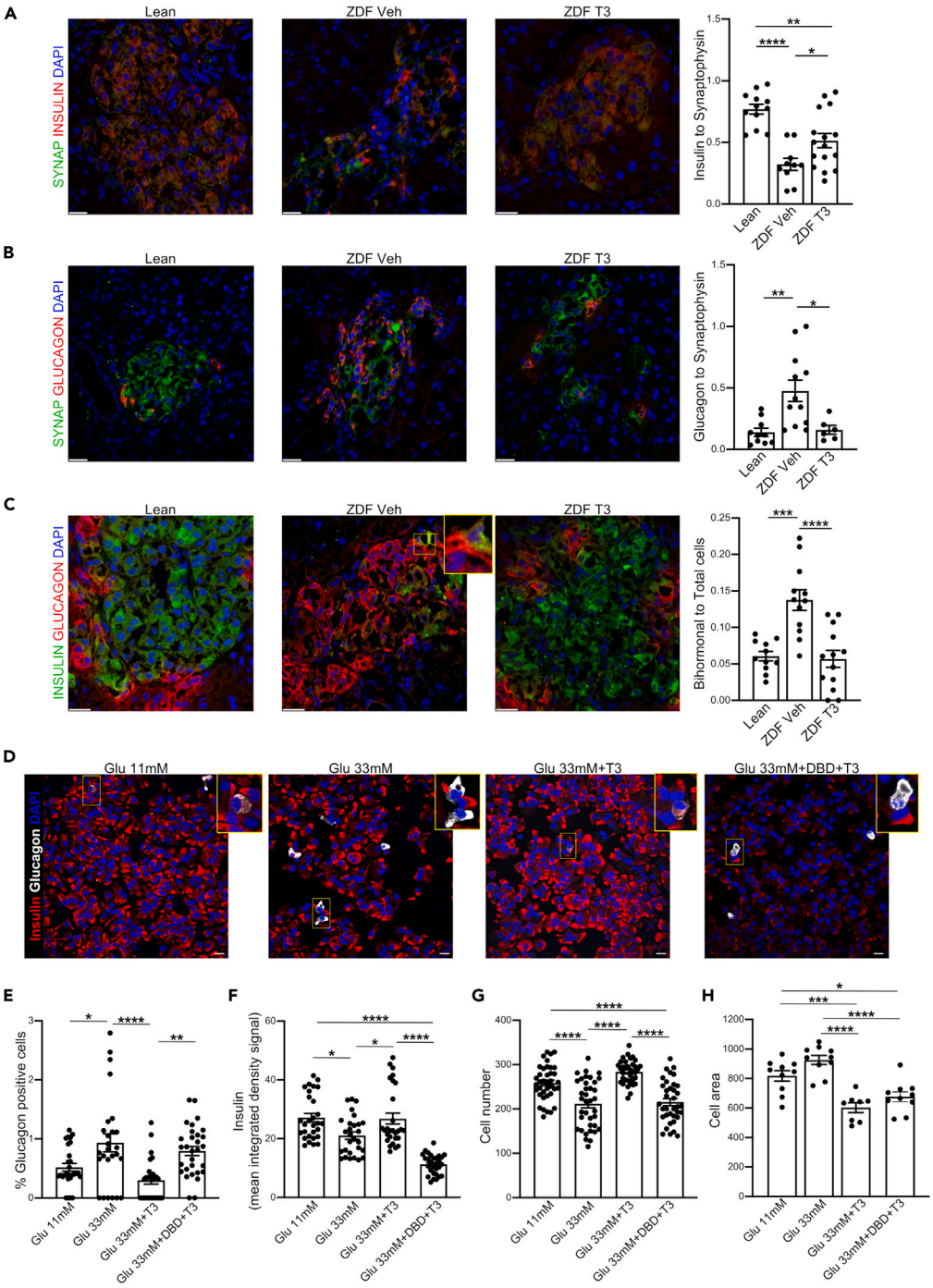

Figure 5. T3 administration prevents pancreatic beta cell transdifferentiation *in vivo* and *in vitro*

(A–C) Representative images of synaptophysin and insulin (A), synaptophysin and glucagon (B), and insulin and glucagon (C) double immunostaining in pancreatic islets of lean and diabetic rats (A–C, left panels). Quantification of insulin (A, right) and glucagon (B, right) to synaptophysin-positive area, and of the number of bihormonal cells to total cell number (C, right). Inset shows enlarged image of a bihormonal cell in a ZDF rat (C).

(D) Representative images of insulin and glucagon staining in human beta cells. Insets show enlarged images of beta cells expressing insulin and glucagon.

(E–H) Quantification of glucagon-positive cells on total cells per field (E), intracellular insulin content (F), cell number (G), and cell area (H) in human pancreatic beta cells. For quantification, representative images were randomly taken from different areas of cell culture. At least 5 fields of each group were analyzed from n = 3/4 independent experiments (E–G); n = 8–10 different field of each group were analyzed (H). Data are expressed as mean ± SEM, one-way ANOVA corrected with Tukey's post hoc test. *p < 0.05, **p < 0.01, ***p < 0.001, ****p < 0.0001. n = 3 animals per group. Scale bars, 20 μm. Synap, synaptophysin.

STAR★METHODS

Detailed methods are provided in the online version of this paper and include the following:

- KEY RESOURCES TABLE
- RESOURCE AVAILABILITY
  - Lead contact
  - Materials availability
  - Data and code availability
- EXPERIMENTAL MODEL AND STUDY PARTICIPANT DETAILS
  - Animals
  - Cell lines
- METHOD DETAILS
  - *In vivo* studies
  - *In vitro* studies
- QUANTIFICATION AND STATISTICAL ANALYSIS

SUPPLEMENTAL INFORMATION

Supplemental information can be found online at https://doi.org/10.1016/j.isci.2023.107826.

ACKNOWLEDGMENTS

The authors are grateful to Kerstin Mierke for the excellent editing work on the manuscript. This research was partially funded by the European Foundation for the Study of Diabetes (EFSD)/Novo Nordisk, Euronanomed (an ERA-NET grant, EURONANOMED2019-049/REASON), Associazione per la Ricerca sul Diabete Italia (ARDI), and Fondazione Telethon. A.M.L. and D. Cerullo are recipients of fellowships from Fondazione Aiuti per la Ricerca sulle Malattie Rare (ARMR), Bergamo (Italy). P.M. was a recipient of a fellowship from Persico s.r.l., Bergamo, Italy.

AUTHOR CONTRIBUTIONS

A.M.L. performed *in vitro* experiments, immunohistochemistry experiments in animals and cultured cells, collected, analyzed, and interpreted the data, prepared the figures, and prepared the manuscript; P.M. performed western blot and immunohistochemistry experiments in animals, collected, analyzed, and interpreted the data, prepared the figures, and drafted the manuscript; D. Cerullo and D. Corna performed animal studies; M.L. performed immunohistochemistry experiments in animals; S.C. and M.T. performed TEM and SEM analysis; F.S. optimized confocal microscopy methods and protocol for morphological studies and DNA content analysis; C.Z. supervised animal studies; G.R. critically revised the manuscript and approved the final version of the manuscript; C.X. conceived and designed the experiments, analyzed and interpreted data, wrote the manuscript, and supervised the study. All authors have read and approved the manuscript. Verification of the underlying data: A.M.L. and C.X.

DECLARATION OF INTERESTS

A.M.L. and C.X. are inventors of a filled patent relating to the development of thyroid hormone-nanocarriers for the treatment of diabetic cardiomyopathy and diabetic nephropathy.

INCLUSION AND DIVERSITY

We support inclusive, diverse, and equitable conduct of research.

Received: June 2, 2023
Revised: July 24, 2023
Accepted: September 1, 2023
Published: September 7, 2023

REFERENCES

1. NCD Risk Factor Collaboration NCD-RisC (2016). Worldwide trends in diabetes since 1980: a pooled analysis of 751 population-based studies with 4.4 million participants. Lancet *387*, 1513–1530. https://doi.org/10.1016/S0140-6736(16)00618-8.
2. Alicic, R.Z., Rooney, M.T., and Tuttle, K.R. (2017). Diabetic Kidney Disease: Challenges, Progress, and Possibilities. Clin. J. Am. Soc. Nephrol. *12*, 2032–2045. https://doi.org/10.2215/CJN.11491116.
3. Matheus, A.S.d.M., Tannus, L.R.M., Cobas, R.A., Palma, C.C.S., Negrato, C.A., and Gomes, M.d.B. (2013). Impact of diabetes on cardiovascular disease: an update. Int. J. Hypertens. *2013*, 653789. https://doi.org/10.1155/2013/653789.
4. Gourdy, P., Darmon, P., Dievart, F., Halimi, J.-M., and Guerci, B. (2023). Combining glucagon-like peptide-1 receptor agonists (GLP-1RAs) and sodium-glucose cotransporter-2 inhibitors (SGLT2is) in patients with type 2 diabetes mellitus (T2DM).

Cardiovasc. Diabetol. *22*, 79. https://doi.org/10.1186/s12933-023-01798-4.

5. Bosch, J., Lonn, E., Pogue, J., Arnold, J.M.O., Dagenais, G.R., and Yusuf, S.; HOPE/HOPE-TOO Study Investigators (2005). Long-term effects of ramipril on cardiovascular events and on diabetes: results of the HOPE study extension. Circulation *112*, 1339–1346. https://doi.org/10.1161/CIRCULATIONAHA.105.548461.
6. Ruggenenti, P., Fassi, A., Ilieva, A.P., Bruno, S., Iliev, I.P., Brusegan, V., Rubis, N., Gherardi, G., Arnoldi, F., Ganeva, M., et al. (2004). Preventing microalbuminuria in type 2 diabetes. N. Engl. J. Med. *351*, 1941–1951. https://doi.org/10.1056/NEJMoa042167.
7. Parving, H.H., Brenner, B.M., Cooper, M.E., de Zeeuw, D., Keane, W.F., Mitch, W.E., Remuzzi, G., Snapinn, S.M., Zhang, Z., and Shahinfar, S. (2001). [Effect of losartan on renal and cardiovascular complications of patients with type 2 diabetes and nephropathy]. Ugeskr. Laeger *163*, 5514–5519.
8. Perico, N., Amuchastegui, S.C., Colosio, V., Sonzogni, G., Bertani, T., and Remuzzi, G. (1994). Evidence that an angiotensin-converting enzyme inhibitor has a different effect on glomerular injury according to the different phase of the disease at which the treatment is started. J. Am. Soc. Nephrol. *5*, 1139–1146.
9. Strauss, M.H., and Hall, A.S. (2006). Angiotensin receptor blockers may increase risk of myocardial infarction: unraveling the ARB-MI paradox. Circulation *114*, 838–854. https://doi.org/10.1161/CIRCULATIONAHA.105.594986.
10. Benedetti, V., Lavecchia, A.M., Locatelli, M., Brizi, V., Corna, D., Todeschini, M., Novelli, R., Benigni, A., Zoja, C., Remuzzi, G., and Xinaris, C. (2019). Alteration of thyroid hormone signaling triggers the diabetes-induced pathological growth, remodeling, and dedifferentiation of podocytes. JCI Insight *4*, 130249. https://doi.org/10.1172/jci.insight.130249.
11. Depre, C., Young, M.E., Ying, J., Ahuja, H.S., Han, Q., Garza, N., Davies, P.J., and Taegtmeyer, H. (2000). Streptozotocin-induced changes in cardiac gene expression in the absence of severe contractile dysfunction. J. Mol. Cell. Cardiol. *32*, 985–996. https://doi.org/10.1006/jmcc.2000.1139.
12. Moin, A.S.M., and Butler, A.E. (2019). Alterations in Beta Cell Identity in Type 1 and Type 2 Diabetes. Curr. Diabetes Rep. *19*, 83. https://doi.org/10.1007/s11892-019-1194-6.
13. Miettinen, T.P., and Björklund, M. (2016). Cellular Allometry of Mitochondrial Functionality Establishes the Optimal Cell Size. Dev. Cell *39*, 370–382. https://doi.org/10.1016/j.devcel.2016.09.004.
14. Miettinen, T.P., and Björklund, M. (2017). Mitochondrial Function and Cell Size: An Allometric Relationship. Trends Cell Biol. *27*, 393–402. https://doi.org/10.1016/j.tcb.2017.02.006.
15. Lavecchia, A.M., Pelekanos, K., Mavelli, F., and Xinaris, C. (2022). Cell Hypertrophy: A "Biophysical Roadblock" to Reversing Kidney Injury. Front. Cell Dev. Biol. *10*, 854998. https://doi.org/10.3389/fcell.2022.854998.
16. Pantos, C., Xinaris, C., Mourouzis, I., Perimenis, P., Politi, E., Spanou, D., and Cokkinos, D.V. (2008). Thyroid hormone receptor alpha 1: a switch to cardiac cell "metamorphosis". J. Physiol. Pharmacol. *59*, 253–269.
17. Pantos, C., Xinaris, C., Mourouzis, I., Kokkinos, A.D., and Cokkinos, D.V. (2008). TNF-alpha administration in neonatal cardiomyocytes is associated with differential expression of thyroid hormone receptors: a response prevented by T3. Horm. Metab. Res. *40*, 731–734. https://doi.org/10.1055/s-2008-1077096.
18. Pantos, C., Mourouzis, I., Markakis, K., Dimopoulos, A., Xinaris, C., Kokkinos, A.D., Panagiotou, M., and Cokkinos, D.V. (2007). Thyroid hormone attenuates cardiac remodeling and improves hemodynamics early after acute myocardial infarction in rats. Eur. J. Cardio. Thorac. Surg. *32*, 333–339. https://doi.org/10.1016/j.ejcts.2007.05.004.
19. Nam, S.M., Kim, Y.N., Yoo, D.Y., Yi, S.S., Choi, J.H., Hwang, I.K., Seong, J.K., and Yoon, Y.S. (2013). Hypothyroidism affects astrocyte and microglial morphology in type 2 diabetes. Neural Regen. Res. *8*, 2458–2467. https://doi.org/10.3969/j.issn.1673-5374.2013.26.007.
20. Blanco-Molina, A., González-Reyes, J.A., Torre-Cisneros, J., López-Miranda, J., Nicolás, M., and Pérez-Jiménez, F. (1991). Effects of hypothyroidism on the ultrastructure of rat pancreatic acinar cells: a stereological analysis. Histol. Histopathol. *6*, 37–42.
21. Janssen, R., Muller, A., and Simonides, W.S. (2017). Cardiac Thyroid Hormone Metabolism and Heart Failure. Eur. Thyroid J. *6*, 130–137. https://doi.org/10.1159/000469708.
22. Pantos, C., Mourouzis, I., Xinaris, C., Papadopoulou-Daifoti, Z., and Cokkinos, D. (2008). Thyroid hormone and "cardiac metamorphosis": potential therapeutic implications. Pharmacol. Ther. *118*, 277–294. https://doi.org/10.1016/j.pharmthera.2008.02.011.
23. Wu, J., Li, X., Tao, Y., Wang, Y., and Peng, Y. (2015). Free Triiodothyronine Levels Are Associated with Diabetic Nephropathy in Euthyroid Patients with Type 2 Diabetes. Internet J. Endocrinol. *2015*, 204893. https://doi.org/10.1155/2015/204893.
24. Razeghi, P., Young, M.E., Cockrill, T.C., Frazier, O.H., and Taegtmeyer, H. (2002). Downregulation of myocardial myocyte enhancer factor 2C and myocyte enhancer factor 2C-regulated gene expression in diabetic patients with nonischemic heart failure. Circulation *106*, 407–411.
25. Mourouzis, I., Lavecchia, A.M., and Xinaris, C. (2020). Thyroid Hormone Signalling: From the Dawn of Life to the Bedside. J. Mol. Evol. *88*, 88–103. https://doi.org/10.1007/s00239-019-09908-1.
26. Mantzouratou, P., Lavecchia, A.M., Novelli, R., and Xinaris, C. (2020). Thyroid Hormone Signalling Alteration in Diabetic Nephropathy and Cardiomyopathy: a "Switch" to the Foetal Gene Programme. Curr. Diabetes Rep. *20*, 58. https://doi.org/10.1007/s11892-020-01344-6.
27. Bensley, J.G., De Matteo, R., Harding, R., and Black, M.J. (2016). Three-dimensional direct measurement of cardiomyocyte volume, nuclearity, and ploidy in thick histological sections. Sci. Rep. *6*, 23756. https://doi.org/10.1038/srep23756.
28. Pantos, C., Xinaris, C., Mourouzis, I., Malliopoulou, V., Kardami, E., and Cokkinos, D.V. (2007). Thyroid hormone changes cardiomyocyte shape and geometry via ERK signaling pathway: potential therapeutic implications in reversing cardiac remodeling? Mol. Cell. Biochem. *297*, 65–72. https://doi.org/10.1007/s11010-006-9323-3.
29. Bishop, S.P., Zhang, J., and Ye, L. (2022). Cardiomyocyte Proliferation from Fetal- to Adult- and from Normal- to Hypertrophy and Failing Hearts. Biology *11*, 880. https://doi.org/10.3390/biology11060880.
30. Liu, J., Lang, G., and Shi, J. (2021). Epigenetic Regulation of PDX-1 in Type 2 Diabetes Mellitus. Diabetes Metab. Syndr. Obes. *14*, 431–442. https://doi.org/10.2147/DMSO.S291932.
31. Ghiraldini, F.G., Crispim, A.C.V., and Mello, M.L.S. (2013). Effects of hyperglycemia and aging on nuclear sirtuins and DNA damage of mouse hepatocytes. Mol. Biol. Cell *24*, 2467–2476. https://doi.org/10.1091/mbc.E13-04-0186.
32. Cabrera, O., Berman, D.M., Kenyon, N.S., Ricordi, C., Berggren, P.-O., and Caicedo, A. (2006). The unique cytoarchitecture of human pancreatic islets has implications for islet cell function. Proc. Natl. Acad. Sci. USA *103*, 2334–2339. https://doi.org/10.1073/pnas.0510790103.
33. Mourouzis, I., Kostakou, E., Galanopoulos, G., Mantzouratou, P., and Pantos, C. (2013). Inhibition of thyroid hormone receptor α1 impairs post-ischemic cardiac performance after myocardial infarction in mice. Mol. Cell. Biochem. *379*, 97–105. https://doi.org/10.1007/s11010-013-1631-9.
34. Zou, J., Tian, F., Zhang, Y., Li, Z., Yang, C., Chen, H., Zhai, J., Shi, M., Xu, C., Zhang, J., et al. (2018). Association between Thyroid Hormone Levels and Diabetic Kidney Disease in Euthyroid Patients with Type 2 Diabetes. Sci. Rep. *8*, 4728. https://doi.org/10.1038/s41598-018-22904-7.
35. Wu, P. (2007). Thyroid disorders and diabetes. It is common for a person to be affected by both thyroid disease and diabetes. Diabetes Self Manag. *24*, 80-2–85-7.
36. Heyland, A., Reitzel, A.M., and Hodin, J. (2004). Thyroid hormones determine developmental mode in sand dollars (Echinodermata: Echinoidea). Evol. Dev. *6*, 382–392. https://doi.org/10.1111/j.1525-142X.2004.04047.x.
37. Laudet, V. (2011). The origins and evolution of vertebrate metamorphosis. Curr. Biol. *21*, R726–R737. https://doi.org/10.1016/j.cub.2011.07.030.
38. Forhead, A.J., and Fowden, A.L. (2014). Thyroid hormones in fetal growth and prepartum maturation. J. Endocrinol. *221*, R87–R103. https://doi.org/10.1530/JOE-14-0025.
39. Mantzouratou, P., Lavecchia, A.M., and Xinaris, C. (2021). Thyroid Hormone Signalling in Human Evolution and Disease: A Novel Hypothesis. J. Clin. Med. *11*, 43. https://doi.org/10.3390/jcm11010043.
40. Chen, C., Xie, Z., Shen, Y., and Xia, S.F. (2018). The Roles of Thyroid and Thyroid Hormone in Pancreas: Physiology and Pathology. Internet J. Endocrinol. *2018*, 2861034. https://doi.org/10.1155/2018/2861034.
41. Mastracci, T.L., and Evans-Molina, C. (2014). Pancreatic and Islet Development and Function: The Role of Thyroid Hormone. J. Endocrinol. Diabetes Obes. *2*, 1044.
42. Aguayo-Mazzucato, C., Zavacki, A.M., Marinelarena, A., Hollister-Lock, J., El Khattabi, I., Marsili, A., Weir, G.C., Sharma, A., Larsen, P.R., and Bonner-Weir, S. (2013). Thyroid hormone promotes postnatal rat

pancreatic β-cell development and glucose-responsive insulin secretion through MAFA. Diabetes *62*, 1569–1580. https://doi.org/10.2337/db12-0849.

43. Pantos, C.I., Trikas, A.G., Pissimisis, E.G., Grigoriou, K.P., Stougiannos, P.N., Dimopoulos, A.K., Linardakis, S.I., Alexopoulos, N.A., Evdoridis, C.G., Gavrielatos, G.D., et al. (2022). Effects of Acute Triiodothyronine Treatment in Patients with Anterior Myocardial Infarction Undergoing Primary Angioplasty: Evidence from a Pilot Randomized Clinical Trial (ThyRepair Study). Thyroid *32*, 714–724. https://doi.org/10.1089/thy.2021.0596.
44. Pantos, C., Kostopanagiotou, G., Armaganidis, A., Trikas, A., Tseti, I., and Mourouzis, I. (2020). Triiodothyronine for the treatment of critically ill patients with COVID-19 infection: A structured summary of a study protocol for a randomised controlled trial. Trials *21*, 573. https://doi.org/10.1186/s13063-020-04474-0.
45. Khin, P.-P., Lee, J.-H., and Jun, H.-S. (2021). A Brief Review of the Mechanisms of β-Cell Dedifferentiation in Type 2 Diabetes. Nutrients *13*, 1593. https://doi.org/10.3390/nu13051593.
46. Honzawa, N., and Fujimoto, K. (2021). The Plasticity of Pancreatic β-Cells. Metabolites *11*, 218. https://doi.org/10.3390/metabo11040218.
47. Lin, Y., and Sun, Z. (2011). Thyroid hormone ameliorates diabetic nephropathy in a mouse model of type II diabetes. J. Endocrinol. *209*, 185–191. https://doi.org/10.1530/JOE-10-0340.
48. Evron, J.M., Hummel, S.L., Reyes-Gastelum, D., Haymart, M.R., Banerjee, M., and Papaleontiou, M. (2022). Association of Thyroid Hormone Treatment Intensity With Cardiovascular Mortality Among US Veterans. JAMA Netw. Open *5*, e2211863. https://doi.org/10.1001/jamanetworkopen.2022.11863.
49. Papaleontiou, M., Levine, D.A., Reyes-Gastelum, D., Hawley, S.T., Banerjee, M., and Haymart, M.R. (2021). Thyroid Hormone Therapy and Incident Stroke. J. Clin. Endocrinol. Metab. *106*, e3890–e3900. https://doi.org/10.1210/clinem/dgab444.
50. Lindsay, R.S., and Toft, A.D. (1997). Hypothyroidism. Lancet *349*, 413–417. https://doi.org/10.1016/S0140-6736(97)80050-5.
51. Saleem, M.A., O'Hare, M.J., Reiser, J., Coward, R.J., Inward, C.D., Farren, T., Xing, C.Y., Ni, L., Mathieson, P.W., and Mundel, P. (2002). A conditionally immortalized human podocyte cell line demonstrating nephrin and podocin expression. J. Am. Soc. Nephrol. *13*, 630–638.
52. Imberti, B., Tomasoni, S., Ciampi, O., Pezzotta, A., Derosas, M., Xinaris, C., Rizzo, P., Papadimou, E., Novelli, R., Benigni, A., et al. (2015). Renal progenitors derived from human iPSCs engraft and restore function in a mouse model of acute kidney injury. Sci. Rep. *5*, 8826. https://doi.org/10.1038/srep08826.
53. Freedman, B.S., Brooks, C.R., Lam, A.Q., Fu, H., Morizane, R., Agrawal, V., Saad, A.F., Li, M.K., Hughes, M.R., Werff, R.V., et al. (2015). Modelling kidney disease with CRISPR-mutant kidney organoids derived from human pluripotent epiblast spheroids. Nat. Commun. *6*, 8715. https://doi.org/10.1038/ncomms9715.
54. Zhao, K., Hao, H., Liu, J., Tong, C., Cheng, Y., Xie, Z., Zang, L., Mu, Y., and Han, W. (2015). Bone marrow-derived mesenchymal stem cells ameliorate chronic high glucose-induced β-cell injury through modulation of autophagy. Cell Death Dis. *6*, e1885. https://doi.org/10.1038/cddis.2015.230.

STAR★METHODS

KEY RESOURCES TABLE

REAGENT or RESOURCE	SOURCE	IDENTIFIER
Antibodies		
α-SMA clone 1A4 (Mouse, Cy3-conjugated)	Sigma-Aldrich	Cat#c6198; AB_476856
Pax2 (Rabbit)	Invitrogen	Cat#71-6000; AB_2336046
Six2 (Rabbit)	Proteintech	Cat#11562-1-AP; AB_2189084
Nestin (Mouse)	BD Biosciences	Cat#556309; AB_396354
Insulin (Mouse)	Proteintech	Cat#66198-1-Ig; AB_2881591
Glucagon (Rabbit)	Proteintech	Cat#15954-1-AP; AB_2878200
Glucagon (Guinea pig)	Origene	Cat#TA364393
PDX1 (Rabbit)	Cell Signaling	Cat#5679
NKX6.1(Rabbit)	Novus Biologicals	Cat#NBP1-49672; AB_10011794
cleaved caspase-3	Cell Signaling	Cat#9664
Synaptophysin	Santa Cruz Biotechnology	Cat#sc-17750; AB_628311
DIO3 (Rabbit)	Novus Biologicals	Cat#NBP1-05767; AB_1556282
TRα1 (Rabbit)	Invitrogen	Cat#PA1-211A; AB_325811
Desmin (Rabbit)	Abcam	Cat#ab1520
WT1 (Mouse)	Santa Cruz Biotechnology	Cat#sc-7385; AB_628448
Glepp1 (Mouse)	Millipore	Cat#MABS455
Myosin heavy chain (Mouse)	Abcam	Cat#ab50967; AB_942084
β-myosin heavy chain (Rabbit)	Abcam	Cat#ab17296
SERCA2a (Rabbit)	Badrilla	Cat#A010-20; AB_2631042
Phospholamban (pSER16) (Rabbit)	Badrilla	Cat#A010-12AP
Troponin (Mouse)	Thermo Fisher Scientific	Cat#MA5-12960; AB_11000742
Connexin43 (Rabbit)	Sigma-Aldrich	Cat#C6219; AB_476857
Fibronectin (Rabbit)	Merck Life Science	Cat#AB2040; AB_91212
Podocalyxin (Rabbit)	Novus Biologicals	Cat#NB110-41503; AB_805568
Insulin (Rabbit)	Santa Cruz Biotechnology	Cat#sc-9168; AB_2126540
FITC Donkey Anti-Rabbit IgG (H+L)	Jackson Immuno Research	Cat#711-095-152
Cy3 Donkey Anti-Rabbit IgG (H+L)	Jackson Immuno Research	Cat#711-165-152
FITC Sheep Anti-Mouse IgG (H+L)	Jackson Immuno Research	Cat# 515-095-003
Cy3 Donkey Anti-Mouse IgG (H+L)	Jackson Immuno Research	Cat#715-165-151
Cy3 Donkey Anti-Guinea Pig IgG (H+L)	Jackson Immuno Research	Cat#706-165-148
Chemicals, peptides, and recombinant proteins		
DyLight 649-labeled lens culinaris agglutinin (LCA)	Vector Laboratories	Cat#DL-1048
FITC wheat-germ agglutinin (WGA)	Vector Laboratories	Cat#FL1021
Rhodamine-labelled WGA lectin	Vector Laboratories	Cat#RL1022
FITC-conjugated-phalloidin	Life Technologies	Cat#A12389
FITC-conjugated lotus tetragonolobus lectin	Vector Laboratories	Cat# FL-1321-2
Normal donkey serum	Jackson Immuno Research	Cat# 017-000-121
GFR basement membrane matrix	Corning	Cat#356231
STEMdiff™ Kidney Organoid Kit	Stem Cell Technologies	Cat#05160
B27	Stem Cell Technologies	Cat#12587010
hESC-qualified matrix	Corning	Cat#354277

(*Continued on next page*)

Continued

REAGENT or RESOURCE	SOURCE	IDENTIFIER
STEMdiff™ cardiomyocyte differentiation kit	Stem Cell Technologies	Cat#05010
T3	Sigma-Aldrich	Cat#T6397
Glucose	MilliporeSigma	Cat#G5146
DBD	Toronto Research Chemicals	Cat#D288875
Critical commercial assays		
ELISA T3	Accubind, Monobind Inc	Cat#125-300
ELISA T4	Accubind, Monobind Inc	Cat#225-300
ELISA TSH	BioVendor LLC	Cat#RTC007R
DC protein assay	Bio-Rad Laboratories	Cat#5000116
Experimental models: Cell lines		
Immortalized human podocytes	Saleem et al.[51]	N/A
EndoC-βH5, human pancreatic beta cells	Human Cell Design	N/A
hiPSCs (clone IV)	Imberti et al.[52]	RRID:CVCL_IT61
Experimental models: Organisms/strains		
Zucker Diabetic Fatty rats (ZDF/Gmi-fa/fa)	Charles River Laboratories	N/A
Non-diabetic lean rats (ZDF/Gmi-fa/+)	Charles River Laboratories	N/A
Software and algorithms		
ImageJ/Fiji software	v 2.3 ImageJ, imagej.net/software/fiji/	RRID:SCR_002285
Graph Pad Prism software 8	http://www.graphpad.com/	RRID:SCR_002798

RESOURCE AVAILABILITY

Lead contact

Further information and requests for resources and reagents should be directed to and will be fulfilled by the lead contact, Christodoulos Xinaris (christodoulos.xinaris@marionegri.it).

Materials availability

This study did not generate new unique reagents.

Data and code availability

- Experimental data reported in this paper will be shared by the lead contact upon request.
- This paper does not report original code.
- Any additional information required to reanalyze the data reported in this paper is available from the lead contact upon request.

EXPERIMENTAL MODEL AND STUDY PARTICIPANT DETAILS

Animals

Male Zucker Diabetic Fatty rats (ZDF/Gmi-fa/fa) and age-matched non-diabetic lean rats (ZDF/Gmi-fa/+) were obtained from Charles River Laboratories Italia (Lecco, Italy). Animals were maintained in a specific pathogen-free facility and kept on a 12:12-h light-dark cycle with free access to water. To accelerate the onset of diabetes and renal complications (Figure S3) ZDF rats were fed with the animal Purina 5008 diet (Charles River) containing 18 kJ% fat. At 10 weeks of age, when ZDF rats develop marked proteinuria, animals were randomly divided into two groups (n=10/group): ZDF rats that received vehicle (ZDF Veh) or T3 (ZDF T3) in their daily drinking water. T3 (Cat#T6397, Sigma-Aldrich) was administered at a dose starting from 6 μg/kg, which was increased to 20 μg/kg during the study.[50] Lean rats (n=10) were followed for the same length of time as controls. All rats were sacrificed at 28 weeks of age and tissues were collected for the following analysis. Twenty-four-hour urine samples were collected using metabolic cages and urinary protein excretion was measured using the Coomassie method, with a Miura one auto-analyzer (I.S.E. S.r.l. Rome, Italy). Fasting blood glucose levels were assessed with a reflectance meter (On Call Plus II, Acon Laboratories Inc., CA, USA).

All procedures involving animals were performed with the approval of and in accordance with internal institutional guidelines of the Istituto di Ricerche Farmacologiche Mario Negri IRCCS, which are in compliance with national (D.L.n.26, March 4, 2014) and international laws and policies (directive 2010/63/EU on the protection of animals used for scientific purposes).

Cell lines

Podocytes

Conditionally immortalized human podocytes were generated[51] and generously provided by Prof Mathieson and Prof Saleem from the Children's Renal Unit and Academic Renal Unit at the University of Bristol.

Human induced pluripotent stem cell (hiPSCs)

Human-derived cardiomyocytes, cardiac and kidney organoids were obtained using hiPSCs (clone IV; RRID:CVCL_IT61).[52]

Pancreatic cells

Human EndoC-βH5® cells (obtained from Human Cell Design) were employed to model glucose injury in beta pancreatic cells.

Details on cell culture and treatment methods are provided below.

METHOD DETAILS

In vivo studies

Thyroid hormone measurements

Fasting serum total triiodothyronine (T3, ng/dl), total thyroxine (T4, μg/ml) and thyroid stimulating hormone (TSH, ng/ml) levels were measured using the appropriate ELISA kit (T3, Cat#125-300, Accubind ELISA Microwells, Monobind Inc; T4, Cat#225-300, Accubind; TSH Cat#RTC007R, BioVendor LLC, Asheville, North Carolina, USA), according to the provider's instructions.

Histological analyses

Histological analysis of renal tissue. Kidneys were fixed overnight in Duboscq-Brazil, dehydrated in alcohol, and embedded in paraffin. Renal sections (3-μm) were stained with periodic acid-Schiff reagent (PAS) (Bio Optica, Milan, Italy),[10] to analyze glomerular injury. At least 50 glomeruli were examined for each animal, and the degree of glomerular damage was assessed using a semi-quantitative scoring method (index) based on the number of glomeruli with sclerosis. Grade 0 normal glomeruli, grade 1 up to 25% involvement, grade 2 up to 50% involvement, grade 3 up to 75%, and grade 4 greater than 75% sclerosis. The indexes were calculated as:

$[(1 \times N1) + (2 \times N2) + (3 \times N3) + (4 \times N4)]/(N0 + N1 + N2 + N3 + N4)$, where Nx is the number of glomeruli in each grade of glomerulosclerosis. Kidney biopsies were analyzed by the same pathologist, who was blind to treatment groups. Samples were examined using ApoTome Axio Imager Z2 (Zeiss, Oberkochen, Germany).

Analysis of heart tissue. Fibrosis was examined in paraffin-embedded heart sections (5-μm) with PicroSirius red staining. The percentage of the total area positive for Sirius red was quantified in 15 to 20 fields (HPF, 20X) per animal using ImageJ software. Digitized images were dichotomized using a threshold for Sirius red staining, and the values were expressed as the percentage of positive area per total field area.

Histological analysis of pancreas tissue. Pancreases were fixed in Bouin for at least 24 hours, embedded in paraffin blocks, and then sectioned (5-μm). Masson's trichrome staining was used to localize the collagen fibers in the pancreas tissue and analyze their distribution around pancreatic islets.

Immunohistochemical analyses

Immunofluorescence analysis was performed as previously described.[10] Briefly, OCT-frozen kidney and pancreas sections (3 μm) were fixed with 4% paraformaldehyde (PFA) (Cat#157-8, Electron Microscopy Sciences) for 10 minutes at RT. After antigen retrieval with 1X citrate buffer pH 7.4 (Cat#C9999, Merck Life Science), sections were blocked with 5% normal donkey serum (NDS) in 1% (w/v) bovine serum albumin (BSA) (Cat#A7906, Sigma-Aldrich, St. Louis, MO, USA) for 1 hour at RT and incubated overnight at 4°C with the following primary antibodies: Cy3-conjugated mouse anti-α-smooth muscle actin (α-SMA) (Cat#c6198, clone 1A4, Sigma-Aldrich, 1:200), rabbit anti-Pax2 (Cat#71-6000, Invitrogen, 1:200), rabbit anti-Six2 (Cat#11562-1-AP, Proteintech, Manchester, UK, 1:200) and mouse anti-rat nestin (Cat#556309, BD Biosciences, USA, CA, 1:100) for kidney sections; or mouse anti-insulin (Cat#66198-1-Ig, Proteintech, 1:100), rabbit anti-glucagon (cat#15954-1-AP, Proteintech, 1:100), guinea pig anti-glucagon (Cat#TA364393, Origene Technologies, Rockville, USA, 1:1000), rabbit anti-PDX1 (Cat#5679, Cell Signaling, 1:200), rabbit anti-NKX6.1 (Cat#NBP1-49672, Novus Biologicals, 1:200), rabbit anti-cleaved caspase-3 (Cat#9664, Cell Signaling, 1:100) and rabbit anti-Synaptophysin (Cat#sc-17750, Santa Cruz Biotechnology, 1:200) for pancreatic samples. After washing with PBS, sections were incubated with Cy3- or FITC-conjugated secondary antibodies (Cat#711-095-152, Cat#711-165-152, Cat# 515-095-003, Cat#715-165-151, Cat#706-165-148, Jackson Immuno Research Laboratories, 1:100) as appropriate for 1 hour at RT. Renal structures were stained with DyLight 649-labeled lens culinaris agglutinin (LCA) or fluorescein-conjugated wheat-germ agglutinin (WGA) (Cat#DL1048, Cat#FL1021, Vector Laboratories, Burlingame, CA, 1:400). Nuclei were stained with DAPI (Cat#D9542, Sigma-Aldrich, 1 μg/ml). Slides were mounted with Dako fluorescent mounting medium (Cat#S302380-2, Agilent Technologies, Santa Clara, CA) and analysed using an inverted confocal laser microscope (Leica TCS SP8, Leica Biosystems). Negative controls were obtained by omitting the primary antibody on adjacent

sections. The quantification of glomerular α-SMA was obtained by calculating the percentage of glomeruli with α-SMA positive cells. At least 20-40 glomeruli/section per animal were randomly analyzed.

Immunohistochemistry. Paraffin-embedded kidney and left ventricle sections (3-μm) were first subjected to antigen retrieval in a decloaking chamber with DIVA buffer (Cat#DV2004MX, Bio Optica) and then incubated with Peroxidazed 1 (Cat#RD913M, Biocare Medical) to quench endogenous peroxidase. Sections were then blocked for 30 minutes with Rodent Block R (Cat#RBR962H, Biocare Medical) and incubated with the following primary antibodies: rabbit anti-DIO3 (Cat#NBP1-05767, Novus Biologicals, 1:2000), rabbit anti-TRα1 (Cat#PA1-211A, Invitrogen, 1:300), rabbit anti-desmin (Cat#ab15200, Abcam, 1:2000), mouse anti-WT1 (Cat#sc-7385, Santa Cruz Biotechnology, 1:30) and mouse anti-Glepp1 (Cat#MABS455, Millipore, 1:100). After being washed with PBS, the sections were incubated with the appropriate rabbit or mouse on Rodent HRP-Polymer (Cat#RMR622G, Cat#MRT621G, Bio Optica) for 20 minutes at RT. Diaminobenzidine substrate solution (Cat#BDB2004H, Biocare Medical) was used to develop signal. The slides were counterstained with Mayer's hematoxylin (Cat#MHS80, Bio Optica), mounted with Eukitt mounting medium (Cat#09-00250, Bio Optica) and observed using a light microscope (ApoTome, Axio Imager Z2, Zeiss). To study the glomerular podocyte density and individual podocyte volume, immunostaining of WT1 and Glepp1 was performed on serial kidney sections. Morphometric analysis was performed as previously described[10] to determine the average number of podocytes per glomerulus and the glomerular volume. The mean podocyte volume (Glepp1-positive) per glomerulus was estimated by multiplying the mean glomerular volume by the mean percentage of the Glepp1-positive area. Podocyte number per glomerular tuft was determined through WT1 immunoperoxidase staining, as described above. The mean individual podocyte volume was estimated by dividing the mean Glepp1-positive tuft volume by the mean podocyte number per tuft. Desmin staining was quantified by using a score from 0 to 3 (0, no staining or traces; 1, staining in <25% of the glomerular tuft; 2, staining affecting 26%–50%; 3, staining in >50%). DIO3 staining was quantified using a semi-quantitative score from 0 to 3 (0, no staining or traces; 1, few cells with positive staining; 2, moderate staining in cells of glomerular tuft; 3, strong staining in cells of glomerular tuft). TRα1 staining was quantified using a semi-quantitative score from 0 to 3 (0, no staining or traces; 1, mild staining in the glomerular tuft and negative staining in the Bowman capsule; 2, mild staining in the glomerular tuft and in the Bowman capsule; 3, strong staining in the glomerular tuft and in the Bowman capsule).

Western blot analysis. Western blot analysis was carried out as previously described.[10] Cardiac left ventricles and pancreatic samples were homogenized and lysed in CelLytic MT Cell Lysis Reagent (Cat#C3228, MilliporeSigma) or in NE-PER nuclear and cytoplasmic extraction reagents (Cat#PR78833, Thermo Fisher Scientific) respectively, supplemented with protease (Cat#11836153001, Sigma-Aldrich) and phosphatase (Cat#04906837001, Sigma-Aldrich) inhibitors. DC protein assay (Cat#5000116, Bio-Rad Laboratories) was used to determine protein concentration. 30μg of whole-cell lysates (for cardiac samples) or nuclear lysates (for pancreatic samples) were separated by SDS polyacrylamide gel electrophoresis or 4-12% gradient gel (Cat#M00652, GenScript) and transferred onto nitrocellulose blots (Cat#GE10600001, MilliporeSigma). After blocking of non-specific binding sites with 5% (w/v) BSA (Cat#A7906, Sigma-Aldrich) in Tris Buffered Saline (TBS)-0.1% Tween-20 (Cat#P2287, Sigma-Aldrich) for 1 hour at RT, blots were incubated overnight at 4°C with the following primary antibodies: mouse anti-myosin heavy chain (Cat#ab50967, Abcam, 1:200), rabbit anti-β-myosin heavy chain (Cat#ab172967, Abcam, 1:400), rabbit anti-SERCA2a (Cat#A010-20, Badrilla, 1:5000), rabbit anti-phospholamban (pSER16) (Cat#A010-12AP, Badrilla, 1:2000) for heart samples; or with rabbit anti-PDX1 (Cat#5679, Cell Signaling, 1:1000), rabbit anti-NKX6.1 (Cat#NBP1-49672, Novus Biologicals, 1:1000) for pancreatic lysates. Blots were then incubated for 1 hour at RT with anti-rabbit or anti-mouse horseradish peroxidase-conjugated secondary antibodies, as appropriate (Cat#A6154, Cat#A9044, MilliporeSigma, 1:5000 to 1:20000) and Super Signal West Pico chemiluminescent substrate (Cat#34580, Life Technologies) was used for signal development. Alternatively, blots were incubated with anti-rabbit or anti-mouse infrared dye-conjugated secondary antibody (Cat#FE3680210, Cat#FE30926210, LiCor, 1:5000 to 1:20000) for 1 hour at RT. Odyssey FC Imaging System (LiCor) was used for image acquisition, and Image Studio Lite 5.0 software (LiCor) for quantification of bands using densitometric analysis.

Morphological assessment of cardiomyocytes in vivo. Cardiomyocytes (at least 75 per group) were randomly selected from previously acquired microscopic fields. Analysis of cardiomyocytes' Feret's diameter was carried out using ImageJ/Fiji software (v 2.3 ImageJ, imagej.net/software/fiji/) after outlining the perimeter of each cell.

Assessment of cell polyploidy. In order to quantify ploidy (genome copies per nucleus) in glomerular cells, cardiomyocytes and insulin-producing beta pancreatic cells, we optimized the methods described earlier.[27] After fixing thick OCT-frozen tissue sections in 4% PFA for 10 minutes, they were permeabilized with methanol (Cat#34860, Sigma) for 30 minutes at RT. Kidney and left ventricle sections were then incubated overnight at 4°C with rhodamine-labelled WGA lectin (Cat#RL1022, Vector Laboratories, 1:400) in DAPI (Cat#D9542, Sigma-Aldrich, 1 μg/ml) to visualize cell membranes and stain nuclei, respectively. To visualize DNA content in beta cells, pancreatic sections were incubated overnight at 4°C with rabbit anti-insulin antibody (Cat#sc-9168, Santa Cruz Biotechnology, 1:100) in DAPI (Cat#D9542, Sigma-Aldrich, 1 μg/ml) and, after washing with PBS, incubated for 4 hours at RT with FITC-conjugated donkey anti-rabbit secondary antibody (Cat#711-095-152, Jackson Immuno Research, 1:100). Z-stack images were acquired every 0.8 μm using an inverted confocal microscope (Leica TCS SP8, Leica Biosystems) and analysed using Fiji software. LasX software (Leica Biosystems) was used to obtain three-dimensional (3D) reconstructed images of thick tissue sections.

Transmission electron microscopy (TEM) analysis. Left ventricular and cortical kidney fragments were fixed in 2.5% glutaraldehyde (Cat#340855, Sigma-Aldrich, Darmstadt, Germany) in 0.1 mol/l cacodylate buffer (pH 7.4) (Cat#11652; Electron Microscopy Sciences, Hatfield, PA), washed repeatedly in cacodylate buffer and embedded in Epon resin. Semi-thin sections were stained with toluidine blue in borax and examined using light microscopy. Sections (100–120 nm) were stained with uranyl acetate for morphologic analysis using a Philips Morgagni transmission electron microscope (Morgagni 268D; Philips, Brno, Czech Republic).

Scanning electron microscopy (SEM) analysis. For SEM analysis, specimens of cortical kidney and left ventricular tissue were post-fixed overnight in 2.5% glutaraldehyde (buffered with 0.1 M sodium cacodylate buffer, pH 7.4). Sections were then repeatedly washed in cacodylate buffer and post-fixed in 1% osmium tetroxide for 1 hour. Fixed specimens were dehydrated with increasing concentrations of alcohol. Samples were rinsed with liquid CO_2 with a critical point dryer (CPD 030, BAL-TEC AG, Balzers, Liechtenstein) immediately following complete dehydration. Samples were then mounted on stubs and coated with gold in a sputter coater (Agar Scientific Ltd, Stansted, England). Coated specimens were observed through SEM using secondary electron detection (Supra 55, Zeiss, Oberkochen, Germany). Acceleration voltage was set to 1.5-2.0 kV and enlargement up to 350 kx.

In vitro studies

Podocytes

Conditionally immortalized human podocytes were propagated at 33°C in RPMI-1640 medium (Cat#21875034, Life Technologies, Europe, BV) supplemented with 10% fetal bovine serum (FBS) (Cat#10270106, Life Technologies), 1% insulin-transferrin-selenium (ITS) (Cat#41400045, Life Technologies) and 1% Penicillin/Streptomycin (Pen/Strep) (Cat#15140122, Life Technologies). For cell differentiation, $5x10^3$ cells/cm^2 were seeded onto rat collagen type I-coated wells and cultured at 37°C for 14 days. Before treatment, cells were starved in culture medium supplemented with 2% FBS overnight. Podocytes were then treated with 40 mM glucose for 9 days (Glu) or with 40 mM glucose for 3 days and in combination with 0.1 μM T3 (Glu+T3) for the following 6 days[10] A control group of cells (CTR) was cultured with RPMI-1640 supplemented with 2% FBS.

Cardiomyocytes

STEMdiff™ cardiomyocyte differentiation kit (Cat#05010, Stem Cell Technologies) was used to differentiate human induced pluripotent stem cells (hiPSCs, clone IV; RRID:CVCL_IT61)[52] into cardiomyocytes. Briefly, for cell propagation, hiPSCs were grown in mTeSR1 complete medium (Cat#85850, Stem Cell Technologies) on hESC-qualified (Cat#354277, Corning) matrigel-coated 100 x 20 mm Petri Dishes (Cat#353003, Corning). Medium was changed daily. For cell differentiation, 80%-confluent cells were harvested using accutase (Cat#A1110501, Invitrogen) and seeded at a density of $3x10^5$ cells/well onto hESC-qualified matrigel-coated 12-well plates and cultured in mTeSR1 complete medium for the first 2 days. Once the hiPSCs reach the necessary confluence ($\geq$95%) cells were differentiated following the manufacturer's instruction. Spontaneously beating cells were observed at day 8 of differentiation, while large areas of beating cardiomyocytes were visible from day 10.

At this time point cells were treated with 40 mM glucose for 5 days (Glu) or with 40 mM glucose for 2 days and in combination with 0.1 μM T3 (Glu+T3) for the following 3 days. Another group of cells was cultured with STEMdiff™ medium and used as controls (CTR). For cell area measurements, cells were harvested after treatment and re-plated at a density of $7x10^3$ cells/cm^2 in 12-well plate.

Cardiac organoids

To obtain cardiac organoids, differentiating cardiomyocytes (differentiation day 8) were harvested and seeded at a density of $25x10^3$ cells/well in ultra-low-attachment 96-well microplates (Cat#3474, Corning). Cells were maintained in STEMdiff™ medium for the following 4 days to allow the generation of 3D cardiac tissues, with medium replacement every 2 days. Medium was then shifted to RPMI-1640 supplemented with 2% B27 (Cat#12587010, Life Technologies). Cardiac organoids were treated with 40 mM glucose for 5 days (Glu) or with 40 mM glucose for 2 days and in combination with 0.1 μM T3 (Glu+T3) for the following 3 days. A control group was maintained in RPMI-1640 supplemented with 2% B27 (CTR).

Kidney organoids

Kidney organoids were generated using hiPSCs (clone IV; RRID:CVCL_IT61)[52] with a two-stage differentiation kit (STEMdiff™ Kidney Organoid Kit, Cat#05160, Stem Cell Technologies), which is based on Freedman's differentiation protocol.[53] Briefly, hiPSCs were cultured in mTeSR1 onto growth-factor-reduced (GFR, Cat#356231, Corning) matrigel-coated 100 x 20 mm Petri Dishes (Cat#353003, Corning). For differentiation hiPSCs were harvested using accutase and seeded at a density of $19x10^3$ cells/cm^2 in 96-well microplates (Cat#89626, Ibidi, GmbH) coated with GFR matrigel, and cultured following the manufacturer's instructions. At the end of differentiation, hiPSC-derived kidney organoids were treated with 40 mM glucose for 9 days (Glu) or with 40 mM glucose for 3 days and in combination with 0.1 μM T3 (Glu+T3) for the following 6 days. Another set of organoids was cultured with STEMdiff™ medium and used as a control group (CTR).

Pancreatic cells

Human EndoC-βH5® cells (Human Cell Design) were used for *in vitro* studies on beta pancreatic cells. EndoC-βH5 cells are fully mature human pancreatic beta cells, which exhibit functional and phenotypical features that are very similar to native beta cells. Cells were seeded at a

density of $12x10^4$ or $6x10^4$ cells/well in 96-well microplates (Cat#89626, Ibidi) for immunofluorescence and cell area analysis, respectively. Cells were cultured following the manufacturer's instructions in ULTIβ1® medium for 6 days. Beta cells were then starved with ULTI-ST® medium for 24 hours and treated with 33 mM glucose for 6 days (Glu 33mM)[54] or with 33 mM glucose for 3 days and in combination with 0.1 μM T3 for the following 3 days (Glu 33mM+T3). Another group of cells was treated with 33 μM glucose for 3 days and pre-incubated with 0.5 μM DBD for 2 hours before 0.1 μM T3 was added for the following 3 days (Glu 33mM+DBD+T3). Control cells were treated with 11 mM glucose for 6 days (Glu 11mM).

For all *in vitro* studies, glucose (Cat#G5146, MilliporeSigma) was dissolved in the respective cell culture medium. Likewise, T3 (Cat#T6397, Sigma-Aldrich) was dissolved in NaOH, DBD (Cat#D288875, Toronto Research Chemicals, ON, Canada) was dissolved in methanol, and they were further diluted in the appropriate culture media.

Measurement of cell shape and size

The axis ratio and cell area of cardiomyocytes, podocytes and pancreatic beta cells were analyzed as previously described.[28] At the end of treatment cells were fixed in PFA 4% (Cat#157-8, Electron Microscopy Sciences) for 10 minutes at RT and images of control and treated cells were randomly acquired using an inverted microscope (Primo Vert, Carl Zeiss) equipped with the AxioCam ERc 5s Rev. 2.0. The long to short axis ratio and cell area were analyzed using ImageJ 1.40g software, after outlining the perimeter of each cell. At least 30-100 randomly selected cells were measured from each well.

Immunofluorescence analyses in vitro

For *in vitro* immunohistochemical analyses, all samples were fixed with PFA 4% at the end of treatment.

Cardiac organoids. Samples were permeabilized with 0.2% Triton X-100 (Cat#93418, Sigma-Aldrich) for 10 minutes and incubated with 3% (w/v) BSA (Cat#A7906, Sigma-Aldrich) for 45 minutes at RT to block non-specific binding sites. After washes, organoids were incubated overnight at 4°C with the following primary antibodies: mouse anti-Troponin (Cat#MA5-12960, Thermo Fisher Scientific 1:200), rabbit anti-Connexin43 (Cat#C6219, Sigma-Aldrich, 1:150), rabbit anti-desmin (Cat#ab15200, Abcam, Cambridge, MA, USA, 1:200) and rabbit anti-fibronectin (Cat#AB2040, Merck Life Science, 1:100). After being washed with PBS, cardiac organoids were incubated with the appropriate Cy3- or Cy5-conjugated secondary antibody (Cat#711-165-152, Cat#715-175-150, Cat#715-165-151, Jackson Immuno Research Laboratories, 1:100) for 1 hour at RT. For F-actin staining, organoids were incubated with FITC-conjugated-phalloidin (Cat#A12389, Life Technologies, 1:150) for 45 minutes at RT.

Kidney organoid. Samples were permeabilized with cold (-20°C) methanol (Cat#34860, Sigma-Aldrich) for 20 minutes and treated with 5% normal donkey serum (NDS) (017-000-121, Jackson Immuno Research Laboratories) in PBS-0.2% Triton X-100 (Cat#93418, Sigma-Aldrich) for 1 hour at RT. Organoids were then incubated overnight at 4°C with the following primary antibodies: mouse anti-WT1 (Cat#sc-7385, Santa Cruz Biotechnology, 1:30), rabbit anti-desmin (Cat#ab15200, Abcam, 1:200) and rabbit anti-podocalyxin (Cat#NB110-41503, Novus Biologicals, 1:80) antibodies. After washing with PBS, samples were incubated with the appropriate Cy3- or Cy5-conjugated secondary antibody (Cat#715-165-151, Cat#711-605-152, Jackson ImmunoResearch Laboratories, 1:100) for 1 hour at RT. FITC-conjugated lotus tetragonolobus lectin (LTL, 1:80 overnight at 4°C) (Cat# FL-1321-2, Vector Laboratories) was used to stain tubular structures when needed.

Pancreatic beta cells. EndoC-βH5 cells were permeabilized with 0.1% Triton X-100 (Cat#93418, Sigma-Aldrich) for 15 minutes at RT. After washing with PBS and blocking of non-specific binding sites with 5% NDS (017-000-121, Jackson Immuno Research Laboratories) in 1% (w/v) BSA (Cat#A7906, Sigma-Aldrich) for 1 hour at RT, cells were incubated overnight at 4°C with the following primary antibodies: mouse anti-insulin (Cat#66198-1-Ig, Proteintech, 1:200), rabbit anti-Glucagon (Cat#15954-1-AP, Proteintech, 1:200) and rabbit anti-TRα1 antibody (Cat#PA1-211A, Invitrogen, 1:80). Cells were then washed with PBS and incubated for 1 hour at RT with the appropriate Cy3- or Cy5-conjugated secondary antibody (Cat#715-165-151, Cat#711-165-152, Cat#711-605-152, Jackson ImmunoResearch Laboratories, 1:100). The expression of insulin in pancreatic beta cells was quantified using ImageJ/Fiji software. Digitized images were binarized using a threshold and the values were expressed as mean intensity signal per field (n=6-9 fields from 4 independent wells per group).

QUANTIFICATION AND STATISTICAL ANALYSIS

For sample size determination, we calculated that 10 animal per treatment group would be able to detect the expected reduction in proteinuria, maintaining 80% statistical power. Graph Pad Prism software (Graph Pad, San Diego, CA, USA) was used to perform statistical analysis. All data are expressed as mean ± SEM or in scatter dot plot diagrams. Comparisons were made using one-way ANOVA corrected with Tukey's post hoc test. The correlation between serum T3 levels and blood glucose was determined by linear regression. Statistical significance was set at $p<0.05$. See figures legends for more details on statistics and values used.